

FOBNN: Fast Oblivious Binarized Neural Network Inference

Xin Chen
East China Normal University
Shanghai, China
xinchen@stu.ecnu.edu.cn

Zhili Chen*
East China Normal University
Shanghai, China
zhlichen@sei.ecnu.edu.cn

Benchang Dong
East China Normal University
Shanghai, China
bcdong@stu.ecnu.edu.cn

Shiwen Wei
East China Normal University
Shanghai, China
51265902068@stu.ecnu.edu.cn

Lin Chen
Sun Yat-sen University
Guangzhou, China
chen@lri.fr

Daojing He
Harbin Institute of Technology
Harbin, China
hedaominghit@163.com

ABSTRACT

The superior performance of deep learning has propelled the rise of Deep Learning as a Service, enabling users to transmit their private data to service providers for model execution and inference retrieval. Nevertheless, the primary concern remains safeguarding the confidentiality of sensitive user data while optimizing the efficiency of secure protocols. To address this, we develop a fast oblivious binarized neural network inference framework, FOBNN. Specifically, we customize binarized convolutional neural networks to enhance oblivious inference, design two fast algorithms for binarized convolutions, and optimize network structures experimentally under constrained costs. Initially, we meticulously analyze the range of intermediate values in binarized convolutions to minimize bit representation, resulting in the Bit Length Bounding (BLB) algorithm. Subsequently, leveraging the efficiency of bitwise operations in BLB, we further enhance performance by employing pure bitwise operations for each binary digit position, yielding the Layer-wise Bit Accumulation (LBA) algorithm. Theoretical analysis validates FOBNN's security and indicates up to 2× improvement in computational and communication costs compared to the state-of-the-art method. We demonstrate our framework's effectiveness in RNA function prediction within bioinformatics. Rigorous experimental assessments confirm that our oblivious inference solutions not only maintain but often exceed the original accuracy, surpassing prior efforts.

CCS CONCEPTS

• **Security and privacy** → *Privacy-preserving protocols; Domain-specific security and privacy architectures*; • **Computing methodologies** → *Neural networks*.

KEYWORDS

Garbled circuits, Fast convolutional computation, Oblivious inference, Binarized network

ACM Reference Format:

Xin Chen, Zhili Chen*, Benchang Dong, Shiwen Wei, Lin Chen, and Daojing He. 2024. FOBNN: Fast Oblivious Binarized Neural Network Inference. In *Proceedings of Make sure to enter the correct conference title from your rights confirmation email (CCS '24)*. ACM, New York, NY, USA, 15 pages. <https://doi.org/XXXXXXXX.XXXXXXX>

1 INTRODUCTION

In the realm of artificial intelligence, Deep Neural Networks (DNNs) have revolutionized various application domains, pushing the boundaries of machine perception and comprehension. Their capabilities have expanded from image recognition to natural language processing and beyond, demonstrating remarkable progress. However, the computational demands and energy consumption associated with these sophisticated models often pose significant challenges. This limitation becomes particularly acute when deploying complex DNNs on resource-constrained devices, such as smartphones and IoT devices, which are increasingly prevalent in today's interconnected world.

The recent surge in the popularity of Deep Learning as a Service (DLaaS) has been remarkable. In this framework, service providers leverage extensive private data to train models on their servers and retain ownership of these trained models. Users then submit their data to the service providers' APIs for inference, receiving corresponding analysis results. However, despite facilitating scalability and ease of deployment for deep neural networks on resource-constrained devices, this approach raises privacy concerns as sensitive user information is inevitably disclosed to the service provider, thereby compromising privacy and security.

To address this pressing challenge, the concept of oblivious inference has garnered significant attention. Oblivious inference empowers users to seamlessly execute models maintained by service providers without compromising the privacy of their inputs or inference outcomes. Additionally, it ensures the confidentiality of model parameters, providing an additional layer of security. This approach holds the promise of bolstering privacy and security within DLaaS environments, thereby paving a secure path for the deployment of deep neural networks on resource-constrained devices. By preserving the confidentiality of both users and service providers, oblivious inference represents a significant step forward in enhancing trust and confidence in DLaaS solutions.

Indeed, oblivious inference for DLaaS frequently encounters notable performance overheads due to the utilization of security mechanisms such as garbled circuits. Many multiplications are

Permission to make digital or hard copies of all or part of this work for personal or classroom use is granted without fee provided that copies are not made or distributed for profit or commercial advantage and that copies bear this notice and the full citation on the first page. Copyrights for components of this work owned by others than the author(s) must be honored. Abstracting with credit is permitted. To copy otherwise, or republish, to post on servers or to redistribute to lists, requires prior specific permission and/or a fee. Request permissions from permissions@acm.org.
CCS '24, October 14–18, 2024, Salt Lake City, U.S.A.

© 2024 Copyright held by the owner/author(s). Publication rights licensed to ACM.
ACM ISBN 978-1-4503-XXXX-X/18/06
<https://doi.org/XXXXXXXX.XXXXXXX>

performed with high throughput in deep learning models. However, multiplications are rather costly in the garbled circuits (GC) protocol, but bit-level operations are inexpensive. It is a contradiction in terms. Binarized neural networks (BNNs), which are a subset of Quantized neural networks (QNNs) employing binary values, offer promising methods for compressing trained models. This compression not only enhances computational speed but also helps reduce costs [9, 29]. These BNNs integrate well with garbled circuits to enable oblivious inference with significantly reduced computational expenses [23], due to the costly multiplications that are substituted by XNOR operations, which are known to be free in the GC protocol, in the inference phase.

We introduce FOBNN, a novel framework which provides fast oblivious inference for customized BNNs. It is worth noting that an efficient oblivious inference solution should take into account how the algorithms of deep learning fit into the computation of security protocols. Specifically, the cost of convolutional operations, inherently linear operations, remains a significant hurdle for oblivious inference using GC in BNNs [31], we emphasize that it is crucial to optimize the convolutions to be GC-compatible alternatives. As such, we introduce a hierarchical approach, determining optimal bitwise representations based on the range of intermediate values, thereby compressing space and cutting computational expenses. Additionally, leveraging the efficiency of bitwise operations, we implement layer-wise bit accumulation to further refine the representation and minimize convolution costs. Our approach outperforms the tree-adder structure in terms of computation and communication costs, as validated by comprehensive evaluations across multiple datasets. Notably, our oblivious inference maintains high accuracy while surpassing the tree-adder, which remains the leading method for convolutional computation [23]. Furthermore, we explore network structure optimization and performance enhancement without increasing the costs of secure inference.

We highlight our contributions as follows.

- **FOBNN design.** FOBNN customizes the network Binarization according to the convolutional neural network. Then it translates the operations into corresponding circuits in GC to perform fast oblivious inference. Furthermore, it optimizes the network structures while keeping the cost of secure inference constant.
- **GC-based fast convolutional computation.** We develop two GC-based fast convolutional computation approaches, Bit Length Bounding and Layer-wise Bit Accumulation, to fully utilize the computational space of bitwise representation in GC and converts the convolutions to be GC-compatible alternatives. Our solutions can achieve up to $2\times$ improvement over the state-of-the-art method.
- **FOBNN implementation and application in bioinformatics.** We conduct extensive experiments to evaluate the performance of oblivious inference. Experiments show that our schemes run faster and consume fewer costs while maintaining accuracy.

The remainder of the paper is organized as follows. Section 2 introduces some technical preliminaries. We show the detailed design of our FOBNN framework in Section 3. We present our Bit Length Bounding solution and Layer-wise Bit Accumulation solution for

convolutional computation in Section 4 and Section 5, and analyze the advantages of the computation and communication costs theoretically. Section 6 shows how to perform customized binarized model and network structure optimization exploration. In Section 7, we apply our solutions to implement a secure RNA function prediction and evaluate the performance in terms of accuracy, running time, and communication overhead compared to the state-of-the-art work. Besides, we evaluate different binarized network structures. Section 8 reviews related work briefly. We summarize the paper in Section 9 in the end.

2 PRELIMINARIES

2.1 Binarized Convolutional Neural Networks

A convolutional neural network (CNN) is composed of multiple layers that perform different functions. The output of each layer serves as the input of the next layer. Below we describe the functionality of the different layers.

Linear Layers: The linear layers in a convolutional neural network contain Convolution (CONV) layers and Fully-Connected (FC) layers. The vector dot product operations are performed to compute the outputs in these layers.

Batch Normalization Layers: A batch normalization (BN) layer usually follows a linear layer to normalize the output. The trainable parameters of batch normalization layers are determined in the training process [11].

Activation Layers: An activation function introduces a non-linear transformation while keeping the dimension of the output consistent with the dimension of the input. Sigmoid and ReLU are two commonly used activation functions in a convolutional neural network.

Pooling Layers: The pooling layers are used to reduce the size of outputs. Max-pooling (MP) and Average-pooling are two of the more commonly used pooling methods. We adopt Max-pooling in this paper.

We adopt the idea of binarized neural networks (BNN) [4] to quantize convolutional neural networks. Specifically, we replace Sigmoid or ReLU with Sign activation function, and the weights and activations in our quantized neural networks are constrained to $+1$ or -1 .

2.2 Garbled Circuits

Garbled circuits (i.e., Yao's protocol), or GC in short, is a generic cryptographic tool for secure multiparty computation [15, 30]. In GC, an arbitrary objective function f can be computed based on private inputs held by two parties, without revealing any information about each party's input to the other. Specifically, one holds its private input x_1 , and the other holds x_2 . First one party (i.e., the garbler) prepares a garbled circuit to evaluate $f(x_1, x_2)$ and transmits the garbled circuit, garbled labels on input x_1 , and the output decoding table to the other party (called the evaluator). The evaluator needs to run a 1-out-of-2 oblivious transfer protocol with the garbler [21] to get its garbled labels on input x_2 obliviously. Then the evaluator computes the garbled output with garbled labels of two parties. Finally, the plain output can be decoded by the output decoding table.

The security model we take into account in this paper is the semi-honest adversary model [7]. A semi-honest adversary means that the adversary is honest but curious. Specifically, a semi-honest adversary follows the protocol specification correctly but tries to infer and learn more information from the received messages and their internal state. The cryptographic protocols we employ can achieve security for arbitrary boolean circuits in the presence of semi-honest adversaries [15].

3 THE FOBNN FRAMEWORK

Figure 1 illustrates our FOBNN framework for oblivious inference. We first customize the CNNs into the BNNs, where costly multiplication operations are replaced with XNOR gates which are essentially free in GC. In oblivious inference for BNNs, we propose two fast solutions to convert the convolutions into GC-compatible alternatives: Bit Length Bounding and Layer-wise Bit Accumulation. In addition, we explore network structure optimization. The performance of the different network structures is evaluated by modifying the number of filters and the kernel size while maintaining the same cost.

The most labor-intensive operation in a secure CNN is the design of boolean circuits for the network. To design the circuits efficiently, we first customize the CNN into the binarized neural network in Section 3.1. Then we introduce secure circuit design using garbled circuits in the binarized network in Section 3.2. Section 3.3 describes the security of our FOBNN framework.

3.1 Customized Network Binarization

Secure convolutional neural networks that use garbled circuits will incur the overhead of computation and communication. While binarized neural networks can break through the dilemma. On the one hand, binarized neural networks can reduce the computation overhead compared with traditional convolutional neural networks. On the other hand, binarized neural networks can be effectively combined with garbled circuits for secure computation, thus reducing the communication overhead.

One major shortcoming of binarized neural networks is their low accuracy. To address the challenge, we design the network architecture elaborately. Based on the traditional convolutional neural network model and the requirements of our target model, we carefully design the structure and the parameters of the binarized network, and thus construct the customized binarized neural network. It ensures that the structure of our customized binarized network is closest to the original CNN and that the accuracy is maintained. The general structure of binarized neural networks is depicted in Figure 2. Specifically, the customization can be divided as follows.

Customized Convolution: The weights of convolution layers are restricted to binary values (i.e., either +1 or -1), and there are no bias vectors in each layer. Thus, the primary parameters that we can customize are the number of filters, kernel size, padding, and strides. In the customized binarized networks, we maintain the same kernel size as in the original CNN for 2D convolution or increase it appropriately for 1D convolution, and binarize by adjusting the number of filters and other parameters.

Customized Activation: We replace the conventional activation function (e.g., ReLU) with a binary activation function (i.e.,

Sign). Meanwhile, we add a batch normalization layer followed by a binary activation function.

Customized Pooling: The max-pooling is more suitable for security operations than the average-pooling. Thus, binary max-pooling is adopted to reduce the size of output. The major customizable parameter is the pool size, and the strides remain the same as the pool size by default.

Customized Full-Connected: The full-connected layers (i.e., dense layers) are usually placed in front of the output layer. The weights and the customized parameters are operated similarly in the customized convolution.

We carefully increase the depth of the network and the parameters of each layer, so as to achieve the original accuracy while maintaining a minimal addition of network structure.

3.2 Oblivious Inference

The binarized neural network allows each layer to be computed using a simplified arithmetic circuit. We describe how to translate the function of different layers to their corresponding boolean circuit in this section.

3.2.1 Secure Convolutional Layers. In our binarized network, the inputs and weights of each linear layer and each convolutional layer are binary values, and linear operations of them are realized using the vector dot product (VDP). Therefore, secure linear computations based on garbled circuits (i.e., secure vector dot product operations) can be implemented using XnorPopcount operations [4]. It proceeds as follows.

(1) Encode and XNOR: Element-wise XNOR operations [23] are performed illustrated in Figure 3. The inputs and weights of the convolutional layer in our customized binarized network are constrained to binary values. We consider two binary vectors, the input vector $\mathbf{x} \in \{-1, +1\}^n$ and the weight vector $\mathbf{w} \in \{-1, +1\}^n$. We encode -1 with one bit 0, and +1 with one bit 1 in both vectors. Thus we get two encoded vectors. We then perform the XNOR operation on the two encoded vectors.

(2) Popcount: The sum of the elements in each binarized vector needs to be computed. It is equivalent to counting the number of bits with a value of 1 minus the number of bits with a value of 0 in each equivalent bit vector. Denote the number of bits with a value of 1 in a bit vector by sc . The size of the bit vector is denoted by len . Thus, the number of bits with a value of 1 in the bit vector can be counted by $len - sc$. The output is computed as $sc - (len - sc) = 2 \cdot sc - len$.

We can observe that the most important thing in a secure convolutional computation is to obviously count the number of bits with a value of 1 in the bit vectors. We propose two fast computation solutions to solve the bitcount problem in Section 4 and Section 5.

3.2.2 Secure Binary Activation Function Layers. We take the function $Sign(\cdot)$ as the binary activation function to output +1 or -1. A batch normalization layer is followed by an activation function layer in quantized binary neural networks [32]. Batch normalization is generally used to normalize features and speed up the convergence of a network [11]. The combination of the two layers is realized by a comparison circuit in garbled circuits.

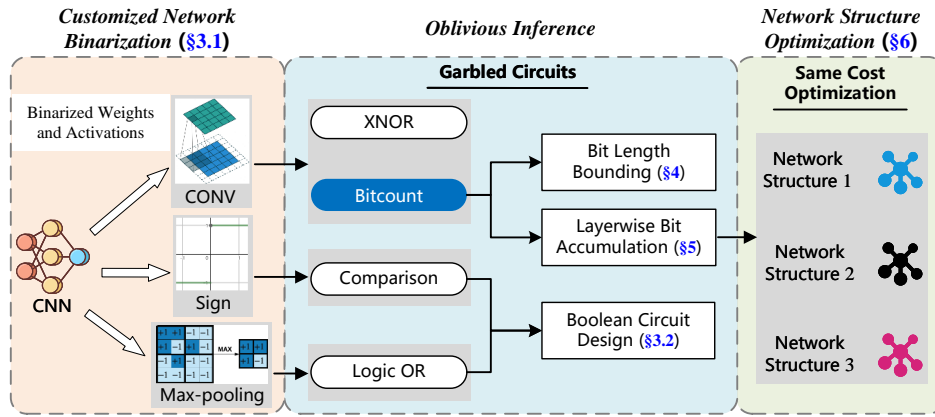


Figure 1: Oblivious inference framework.

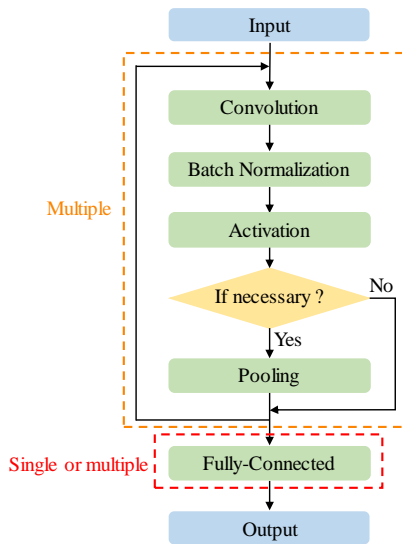


Figure 2: General structure of binarized neural networks.

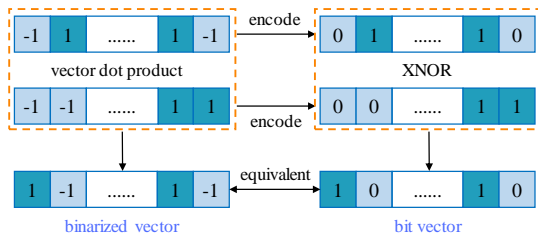


Figure 3: Encode and XNOR operation of two binary vectors.

3.2.3 *Secure Binary Max-pooling Layers.* Since we use max-pooling instead of average-pooling, and the inputs of max-pooling are binarized, the maximum in a pooling window is equivalent to performing logical OR over the binary encodings in garbled circuits.

We can also optimize the binarized network structure while considering the boolean circuit design. We explore modifying different

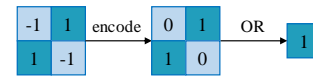


Figure 4: Binary max-pooling operation.

binarized network structures while consuming approximate costs in Section 6.

3.3 Security Analysis

In our FOBNN framework, we tailor the binarized network for CNNs, perform oblivious inference, and conduct network structure optimization. In the whole pipeline process, all the oblivious inference operations of the binarized networks for our FOBNN framework need to be transformed into Boolean circuits, which in turn are converted into garbled circuits. Therefore, the security of the FOBNN framework can be reduced to the security of the garbled circuits.

Our FOBNN framework is constructed using garbled circuits against semi-honest adversaries, which is consistent with other state-of-the-art adversary models for oblivious inference [16, 19, 23, 25]. The parties involved in the model follow the protocol specification correctly but try to infer and learn more information from the received messages and their internal state. Our framework relies on garbled circuits protocols, whose security was proved theoretically in [15]. The oblivious inference of our customized binarized network does not affect the garbled circuits protocol. Specifically, we have converted operations in CNNs into GC-compatible alternatives in our framework, which use as few non-XOR gates as possible in garbled circuits and thus can be computed more efficiently. In oblivious inference of our framework, one party holds the trained model and the other party holds the inputs. As long as the parties do not collude, the party holding the inputs can obtain the inference result without revealing the input to the other party, and the party holding the model will not expose the model parameters. Therefore, our proposed framework preserves privacy against semi-honest adversaries.

4 BIT LENGTH BOUNDING

The convolution operations in traditional convolutional neural networks can be replaced by the XnorPopcount operations in quantized binary neural networks [4]. The XNOR operations are essentially free in garbled circuits protocol [14]. Thus, we first present the motivation for our computation scheme and then design a Bit Length Bounding (BLB) approach for convolutional computation based on garbled circuits and the idea of XnorPopcount. We finally compare with the tree-adder structure in terms of overhead.

4.1 Motivation

As we know, the most important step in the XnorPopcount operations is to obliviously count the number of bits with a value of 1 in the bit vectors. The state-of-the-art solution is to use the tree-adder [23]. They use a way of the inverted binary tree to compute the sum. Specifically, we first analyze the case of summing two 1-bit numbers. Every two 1-bit numbers are added to produce a 2-bit number whose value is at most 2, while the maximum bitwise representation of an unsigned 2-bit number is 11 whose value is 3. Further, the result of adding two 2-bit numbers by a tree-adder has a maximum value of $3 + 3 = 6$, but the maximum value of an unsigned 3-bit number is 7. We can observe that the addition of two n -bit numbers by a tree-adder yields a $(n+1)$ -bit number whose value is at most $2 \cdot (2^n - 1) = 2^{n+1} - 2$, yet the maximum value of an unsigned $(n+1)$ -bit number is $2^{n+1} - 1$. Therefore, the result computed by the tree-adder cannot fill the maximum value of the bitwise representation, which does not make full use of the capacity of bitwise representation, and results in a waste of bit space.

We propose a Bit Length Bounding computation scheme to address the above challenges. The idea is to utilize the target results to backtrack to deduce how many numbers need to be summed and the maximum bitwise representation of the numbers being summed. Specifically, we start by bounding the 2-bit numbers. The maximum value of a 2-bit number is 3, and $3 = 2^2 - 1 = (2^1 + 1)(2^1 - 1) = 3 \cdot (2^1 - 1)$. Since $(2^1 - 1) = 1$ is the maximum value of a 1-bit number, the result of summing three 1-bit numbers just fills the maximum bitwise representation of a 2-bit number. Next, we consider how many 2-bit numbers can be summed to fill the maximum bitwise representation of a 3-bit number. The maximum value of a 2-bit number is $2^2 - 1 = 3$, and the maximum value of a 3-bit number is $2^3 - 1 = 7$, while 7 is not divisible by 3. Therefore, a 3-bit number with maximum value cannot be obtained by summing multiple 2-bit numbers with maximum value. However, we find that multiple 2-bit numbers can fill the maximum bitwise representation of a 4-bit number. The maximum value of a 4-bit number is $2^4 - 1 = 15$, which is exactly divisible by 3, namely, $2^4 - 1 = (2^2 + 1)(2^2 - 1) = 5 \cdot (2^2 - 1)$. Thus, we sum every five 2-bit numbers to compute a 4-bit number. Based on the above analysis, we summarize our computation way: when the inputs to the computation are 2^i -bit numbers, we sum every $2^{2^i} + 1$ numbers to output a 2^{i+1} -bit number. Because the maximum value of a 2^i -bit number and a 2^{i+1} -bit number is $2^{2^i} - 1$ and $2^{2^{i+1}} - 1$ respectively, and $2^{2^{i+1}} - 1 = (2^{2^i} + 1)(2^{2^i} - 1)$.

4.2 BLB Computation

Our BLB solution can obviously acquire the total number of bits in the vector with a value of 1, which is fast and uses less computation

and communication costs. We divide the solution into two steps as follows.

4.2.1 Bit Computation. The inputs in this step are 1-bit numbers and the outputs are 2-bit numbers. Specifically, each element in a bit vector is a 1-bit number, whose max value is either 0 or 1. The maximum unsigned value that can be represented by two bits is 3. Therefore, for each bit vector, we divide every three adjacent elements into a group. The three 1-bit numbers in each group are summed by invoking a 1-bit adder circuit inspired by [13] shown in Figure 5 to produce a 2-bit number. The inputs of a conventional 1-bit adder are two input bits as well as a carry-in bit from the previous 1-bit adder, while our 1-bit adder has three input bits a , b , and c and it can be reused. The outputs are the carry-out bit $d_1 = c \oplus ((a \oplus c) \wedge (b \oplus c))$ and the sum bit $d_0 = a \oplus b \oplus c$. By doing so, we end up with a set of 2-bit numbers for each bit vector.

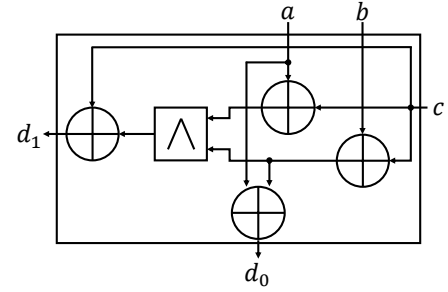


Figure 5: 1-bit Adder.

4.2.2 Cross-layer Computation. Once we obtain the set of 2-bit numbers, we can perform the cross-layer computation iteratively until the count of the number of output elements is one. Considering the input of the cross-layer computation as 2^p -bit numbers. As analyzed in the previous section, the output of the computation is a set of 2^{p+1} -bit numbers. We start by grouping the inputs for each computation, the number of elements in each group is $2^{2^p} + 1$. In each group, we compute the summation of the first 2^{2^p} inputs, level by level, using an inverted binary tree approach: every two elements in the current layer are added using standard GC integer addition to produce a new element in the next layer whose bit length is incremented by one. We compute iteratively until the number of elements in a certain layer is one. A 2^{p+1} -bit number is obtained by summing as described above. Algorithm 1 shows the construction of the inverted binary tree computation. We then sum the remaining 2^p -bit number with it to compute the output of each group. Since we bound the bit number of the inputs and the output in the computation, the output of the computation does not overflow and remains a 2^{p+1} -bit number. Algorithm 2 describes the above details.

Figure 6 illustrates how to perform our BLB computation. The number inside each square indicates the real value represented by one bit. We first divide the target bit vector consisting of fifteen 1-bit numbers (i.e., the values in the grey squares) into five groups of three elements each. A 1-bit adder circuit is invoked in each group to obtain a 2-bit number composed of a carry-out bit and a sum bit. The five sets of values in the blue squares are the real

Algorithm 1 Inverted Binary Tree Calculation

Input: 2^p -bit numbers set $\mathbb{X} = \{x_i\}_{i \in [1..l]}$, $x_i \in \{0, 1\}^p$
Output: A q -bit number S_q

- 1: $q \leftarrow 2^p$
- 2: **while** $l > 1$ **do**
- 3: $\mathbb{X}_1 \leftarrow \emptyset$, $i \leftarrow 1$, $group \leftarrow l/2$, $r \leftarrow l \bmod 2$
- 4: **for** $j = 1$ to $group$ **do**
- 5: $s_j \leftarrow x_i + x_{i+1}$ \triangleright standard GC addition
- 6: $i \leftarrow i + 2$, $\mathbb{X}_1 \leftarrow \mathbb{X}_1 \cup s_j$
- 7: **end for**
- 8: **if** $r = 1$ **then**
- 9: $\mathbb{X}_1 \leftarrow \mathbb{X}_1 \cup x_i$
- 10: **end if**
- 11: $\mathbb{X} \leftarrow \mathbb{X}_1$, $q \leftarrow q + 1$
- 12: **end while**
- 13: **return** x_1

Algorithm 2 Secure Cross-layer Computation for 2^p -bit Numbers

Input: 2^p -bit numbers set $\mathbb{X} = \{x_i\}_{i \in [1..n]}$, $x_i \in \{0, 1\}^{2^p}$
Output: 2^{p+1} -bit numbers set $\mathbb{Y} = \{y_j\}_{j \in [1..n']}$, $y_j \in \{0, 1\}^{2^{p+1}}$ or a q -bit number y_q

- 1: $ct \leftarrow \lceil \frac{n}{2^{2^p} + 1} \rceil$ \triangleright count of groups
- 2: $t \leftarrow 1$
- 3: **if** $n < 2^{2^p} + 1$ **then** \triangleright not enough to form a group
- 4: $S_q \leftarrow Tree(\mathbb{X})$ \triangleright sum by tree via Algorithm 2
- 5: $y_q \leftarrow S_q$
- 6: **return** y_q .
- 7: **end if**
- 8: **for** $j = 1$ to ct **do** \triangleright compute by groups
- 9: $\mathbb{X}_j \leftarrow \{x_i\}_{i \in [t..t+2^{2^p} - 1]}$ \triangleright first 2^{2^p} values in a group
- 10: $S_{2^{p+1}} \leftarrow Tree(\mathbb{X}_j)$ \triangleright sum by tree via Algorithm 2
- 11: $y_j \leftarrow S_{2^{p+1}} + x_{t+2^{2^p}}$ \triangleright y_j is a 2^{p+1} -bit value
- 12: $t \leftarrow t + 2^{2^p} + 1$
- 13: **end for**
- 14: **return** \mathbb{Y} .

numbers computed by *Bit Computation* where each number can be represented by two bits. Then in the *Cross-layer Computation* phase, the first four numbers are summed by an inverted binary tree. Specifically, they are divided into two groups, and two 3-bit numbers (i.e., the values in the purple squares), as well as one 4-bit number (i.e., the values in the green squares), are computed using standard GC integer addition. We end up with a 4-bit number and a remaining 2-bit number which equals 9 and 1 respectively. The sum of the above two numbers does not exceed the maximum value represented by four bits (i.e., 15). Eventually, we obtain a result represented by four bits (i.e., equals 10).

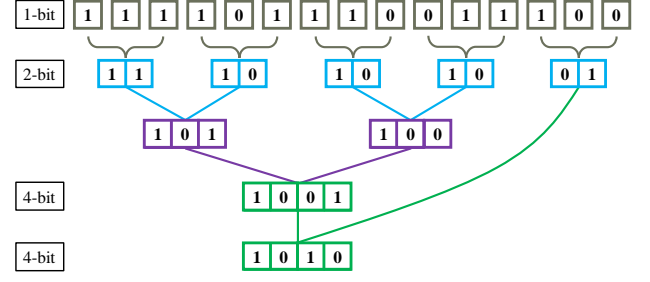


Figure 6: An example of BLB solution.

4.3 Theoretical Analysis of non-XOR Gates

The main overhead of the secure convolutional computation is obviously counting the number of bits with a value of 1 in the bit vectors, so we compare our BLB computation method with the tree-adder structure [23] in terms of the costs consumed. The XOR operation is known to be free in the GC protocol [14]; therefore, we measure the computation and communication costs in GC by non-XOR gates. In this section, we qualitatively analyze the quantity of non-XOR gates required for both. Denote the length of a bit vector by N , and denote the maximum bit length that can represent the result by $L = \lceil \log_2(N + 1) \rceil$. For ease of computation, we uniformly substitute $L = \log_2 N$ for $L = \lceil \log_2(N + 1) \rceil$ in this paper.

LEMMA 4.1. *The number of non-XOR gates consumed for the tree-adder structure is $S_N^{ts} = 2 \cdot (N - 1) - \log_2 N$.*

PROOF. The ℓ -bit adders ($\ell \in [1..L]$) are used to compute the final result in the tree-adder structure. The number of non-XOR gates for each ℓ -bit adder is ℓ , and the number of ℓ -bit adders is $\frac{N}{2^\ell}$. Therefore, the total number of non-XOR gates can be computed as follows.

$$S_N^{ts} = \sum_{\ell=1}^L \left(\frac{N}{2^\ell} \cdot \ell \right) = 2 \cdot (N - 1) - \log_2 N \quad (1)$$

The detailed process of derivation is available in the Appendix A.1. \square

We define $K = \lceil \log_2 \log_2(N + 1) \rceil$.

THEOREM 4.2. *The number of non-XOR gates consumed for our BLB computation is $S_K^{blb} = \sum_{\kappa=1}^{K-1} \left(\frac{N}{\prod_{\ell=0}^{\kappa} (2^{2^\ell} + 1)} \cdot (2^{2^\kappa} \cdot 2^\kappa + 2^{2^\kappa} - 2) \right) + \frac{N}{3}$, and $1.29N < S_K^{blb} < 1.71N$.*

PROOF. Our BLB computation is divided into two steps, and the number of non-XOR gates is also divided into two parts that are counted separately. The number of non-XOR gates in the *Bit Computation* step is $\frac{N}{3}$. In the κ -th *Cross-layer Computation*, the amount of groups is

$$A_\kappa = \frac{N}{\prod_{\ell=0}^{\kappa} (2^{2^\ell} + 1)} \quad (2)$$

and the number of non-XOR gates in each group can be computed by

$$G_\kappa = 2^{2^\kappa} \cdot 2^\kappa + 2^{2^\kappa} - 2. \quad (3)$$

Appendix A.2 shows the derivation process of G_K . Thus, the total number of non-XOR gates in this scheme can be defined as follows.

$$\begin{aligned}
 S_K^{blb} &= \sum_{\kappa=1}^{K-1} (A_\kappa \cdot G_\kappa) + \frac{N}{3} \\
 &= \sum_{\kappa=1}^{K-1} \left(\frac{N}{\prod_{\ell=0}^{\kappa-1} (2^{2^\ell} + 1)} \cdot (2^{2^\kappa} \cdot 2^\kappa + 2^{2^\kappa} - 2) \right) + \frac{N}{3} \\
 &< \sum_{\kappa=1}^{K-1} \left(\frac{N}{\prod_{\ell=0}^{\kappa-1} (2^{2^\ell} + 1) \cdot (2^{2^\kappa} + 1)} \cdot (2^{2^\kappa} + 1) \cdot (2^\kappa + 1) \right) + \frac{N}{3} \\
 &< \frac{N}{3} + \frac{N \cdot 3}{3} + \frac{N \cdot 5}{3 \cdot 5} + \left(\frac{N \cdot 9}{3 \cdot 5 \cdot 17} + \frac{N \cdot 17}{3 \cdot 5 \cdot 17 \cdot 257} + \dots \right) \\
 &< \frac{5N}{3} + \frac{N}{3 \cdot 5 \cdot 17} \cdot (9 + 1) < 1.71N
 \end{aligned}$$

Similarly,

$$\begin{aligned}
 S_K^{blb} &> \sum_{\kappa=1}^{K-1} \left(\frac{N}{\prod_{\ell=0}^{\kappa-1} (2^{2^\ell} + 1) \cdot (2^{2^\kappa} + 1)} \cdot (2^{2^\kappa} + 1) \cdot 2^\kappa \right) + \frac{N}{3} \\
 &= \frac{N}{3} + \frac{N \cdot 2}{3} + \frac{N \cdot 4}{3 \cdot 5} + \frac{N \cdot 8}{3 \cdot 5 \cdot 17} + \frac{N \cdot 16}{3 \cdot 5 \cdot 17 \cdot 257} + \dots
 \end{aligned}$$

if $N > 255$ holds, we have $S_K^{blb} > 1.29N$.

The proof is completed. \square

Consequently, we can conclude that our BLB computation method is superior to the tree-adder structure concerning the number of non-XOR gates that need to be consumed.

5 LAYER-WISE BIT ACCUMULATION

In this section, we analyze the drawback of our BLB computation and propose a Layer-wise Bit Accumulation (LBA) computation based on GC. We analyze the advantages of our LBA solution, compared with the BLB solution and the tree structure computation approach.

5.1 Motivation

Although our BLB computation is sufficiently compact in the bitwise representation, it is limited to the internal computation in a group. We observe that the computational effort from 1-bit numbers to 2-bit numbers is minimal, which means our BLB computation scheme gains the most benefits in *Bit Computation* compared to the tree-adder structure. In the tree-adder structure, each 2-bit number is summed by two 1-bit numbers; whereas in our BLB computation, a 2-bit number can be summed by three 1-bit numbers. Therefore, we consider whether it is possible to use the computation way in *Bit Computation* (i.e., from 1-bit numbers to 2-bit numbers) for all computations.

We propose a Layer-wise Bit Accumulation computation scheme to achieve it. Our design rationale is to perform bit accumulation and computation layer by layer in the bitwise representation. Specifically, we hold a set of 1-bit numbers for each bit vector. Each bit represents a value of 2^0 . We first compute the output of the first layer (i.e., the 2^0 -layer) as follows. Following the method described by *Bit Computation*, we sum every three numbers in the set by the adder in Figure 5 to compute a carry-out bit and a sum bit, which represent a value of 2^1 and 2^0 , respectively. The carry-out bit is

added to the set of the 2^1 -layer, and the sum bit is added to the set of the 2^0 -layer. We perform the above computation continuously until the count of numbers in the set of the 2^0 -layer is one. Thus, we get a set of bits for the 2^1 -layer whose each bit is a value of 2^1 , and the output bit of the 2^0 -layer. We then take the set of the 2^1 -layer as input and utilize a similar way to the computation process of the 2^0 -layer to produce a set of bits for the 2^2 -layer and the output bit of the 2^1 -layer. Further, the set of the 2^2 -layer is used as an input to the next process and is computed iteratively until all bits of the bitwise representations are computed.

5.2 LBA Computation

Our LBA computation solution achieves higher efficiency while using as few non-XOR gates as possible. Algorithm 3 describes the overall structure of the secure layer-wise computation. The input of the algorithm is a bit vector and the output is a vector of q bits. q denotes the minimum number of bits that can represent the result of the target computation. We accumulate and compute all the values of bits in the bitwise representation layer by layer. Next, we will explain in detail how to perform the computations in each layer.

Algorithm 3 Secure Layer-wise Computation

Input: bit vector $\mathbb{X} = \{x_i\}_{i \in [1..n]}$, $x_i \in \{0, 1\}$
Output: q bits vector $\mathbb{Y} = \{y_k\}_{k \in [1..q]}$, $y_k \in \{0, 1\}$

- 1: $\mathbb{X}^C \leftarrow \mathbb{X}, d_0 \in \{0, 1\}, d_1 \in \{0, 1\}, q \leftarrow \lceil \log_2(n+1) \rceil$
- 2: **for** $k = 1$ to q **do** \triangleright layer-wise computation
- 3: $\mathbb{X}^0 \leftarrow \emptyset, \mathbb{X}^1 \leftarrow \emptyset$ $\triangleright \mathbb{X}^C = \{x_t\}_{t \in [1..n]}$
- 4: $group \leftarrow n'/3, r \leftarrow n' \bmod 3$
- 5: **while** $group \geq 1$ **do**
- 6: $t \leftarrow 1$
- 7: **for** $j = 1$ to $group$ **do** \triangleright compute by groups
- 8: $d_1 d_0 \leftarrow adder(x_t, x_{t+1}, x_{t+2})$
- 9: $\mathbb{X}^1 \leftarrow \mathbb{X}^1 \cup \{d_1\}, \mathbb{X}^0 \leftarrow \mathbb{X}^0 \cup \{d_0\}$
- 10: $t \leftarrow t + 3$
- 11: **end for**
- 12: **if** $r = 1$ **then**
- 13: $\mathbb{X}^0 \leftarrow \mathbb{X}^0 \cup \{x_t\}$
- 14: **else if** $r = 2$ **then**
- 15: $\mathbb{X}^0 \leftarrow \mathbb{X}^0 \cup \{x_t, x_{t+1}\}$
- 16: **end if**
- 17: $\mathbb{X}^C \leftarrow \mathbb{X}^0, group \leftarrow n'/3, r \leftarrow n' \bmod 3$
- 18: **end while**
- 19: **if** $r = 1$ **then** $\triangleright \mathbb{X}^C = \{x_0\}$
- 20: $y_k \leftarrow x_0$
- 21: **else if** $r = 2$ **then** $\triangleright \mathbb{X}^C = \{x_0, x_1\}$
- 22: $d_1 d_0 \leftarrow adder(x_0, x_1, 0)$
- 23: $\mathbb{X}^1 \leftarrow \mathbb{X}^1 \cup \{d_1\}, y_k \leftarrow d_0$
- 24: **end if**
- 25: $\mathbb{X}^C \leftarrow \mathbb{X}^1$
- 26: **end for**

We illustrate the computation process of a bit vector \mathbb{X}^C as an example. We first define two empty sets \mathbb{X}^1 and \mathbb{X}^0 to store

the carry-out bits and the sum bits computed by the circuit of Figure 5 respectively. We divide the elements of the bit vector into groups, with every 3 elements divided into a group. As long as the number of groups in the set \mathbb{X}^C is not less than one, we perform the computation as follows iteratively.

- 1) Within each group with three elements, we invoke the 1-bit adder circuit in Figure 5 to obtain a carry-out bit d_1 and a sum bit d_0 (line 8).
- 2) The carry-out bit d_1 and the sum bit d_0 within each group is added to the set \mathbb{X}^1 and the set \mathbb{X}^0 , respectively (line 9).
- 3) All elements in the last group with less than three elements are added to the set \mathbb{X}^0 (line 12-16).
- 4) Assigning the set \mathbb{X}^0 to the set \mathbb{X}^C and updating the relevant parameters of the set \mathbb{X}^C (line 17).

After performing the above operations, the number of elements in the set \mathbb{X}^C will be either one or two (line 19-24). If there is only one element in the set (i.e., $\mathbb{X}^C = \{x_0\}$), this means that the value of the lowest bit (i.e., y_1) is x_0 . Otherwise, the carry-out bit d_1 and the sum bit d_0 are computed by performing the circuit of Figure 5, where the inputs of the circuit are two elements of the set along with 0. d_1 is added to \mathbb{X}^1 , and the lowest bit of the output is d_0 . At this point, all elements in \mathbb{X}^1 are the values of the last but one bit (i.e., the bits of 2^1). We assign \mathbb{X}^1 to \mathbb{X}^C and follow the above computation process to obtain y_2, \dots, y_q .

Once we have the output vector $\mathbb{Y} = \{y_k\}_{k \in [1..q]}$, $y_k \in \{0, 1\}$, we can get the final value computed by $sc = \sum_{k=1}^q y_k \cdot 2^{k-1}$.

Figure 7 demonstrates the computation process of a bit vector consisting of nine elements. Each square in the figure represents a 1-bit value. First, we divide the nine 1-bit values into three groups. Each group is computed using a 1-bit adder circuit depicted in Figure 5 to obtain a carry-out bit and a sum bit, which represents a value of 2^1 and 2^0 respectively. The three computed sum bits form a group and the adder is invoked again to compute a carry-out bit and a sum bit. Thus, we get four 1-bit values of 2^1 and a final value of 2^0 . Second, we divide the four 1-bit values of 2^1 into groups. The first three elements form a group and obtain a carry-out bit and a sum bit, which represents a value of 2^2 and 2^1 , by using the adder. To compute a final value of 2^1 , the adder is invoked again, where the inputs are the remaining element and the sum bit along with an auxiliary 1-bit element which is 0. We hold two values of 2^2 and a final value of 2^1 in this step. Then, we put the two values of 2^2 and a supplementary bit whose value is 0 into a group. The final value of 2^3 and the final value of 2^2 (i.e., the carry-out bit and the sum bit) can be computed by the 1-bit adder circuit. Finally, once we hold the four final values, we can compute the result by $sc = 0 \cdot 2^0 + 1 \cdot 2^1 + 1 \cdot 2^2 + 0 \cdot 2^3 = 6$.

5.3 Theoretical Analysis of non-XOR Gates

In this section, we evaluate the number of non-XOR gates consumed by our LBA computation scheme.

THEOREM 5.1. *The number of non-XOR gates consumed for our LBA computation is S_N^{lba} and $N - \lceil \log_2(N+1) \rceil \leq S_N^{lba} \leq N$.*

PROOF. The 1-bit adder circuit in Figure 5 is reused in our LBA computation solution. Each circuit has an input of three bits and an output of two bits. It means that each time the circuit is executed,

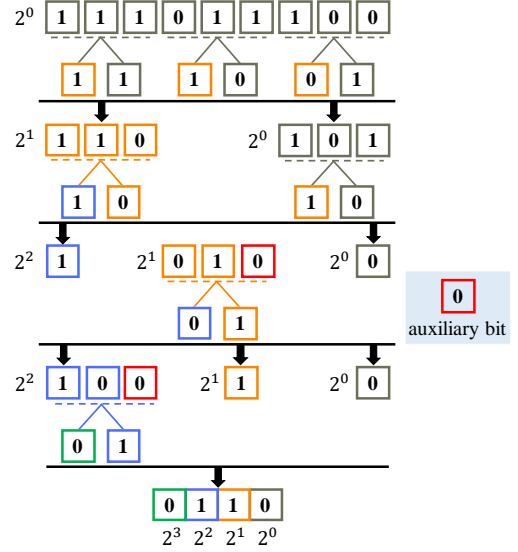


Figure 7: An example of accelerated computation. The values from the least significant bit up to the most significant bit are computed sequentially (i.e., 2^0 to 2^3). The computation of each bit ends up with the remaining number of this bit as one. In each computation, a 1-bit adder is used for every three elements. If the number of elements in the last group of each computation is two, it is computed together with the supplementary bit.

the input is one bit more than the output and the number of non-XOR gates consumed per circuit execution is one. Therefore, we can infer the number of non-XOR gates consumed by our LBA scheme by the difference between the number of bits at the input and output.

The number of bits for input in our LBA solution is N , and the number of output bits is $\lceil \log_2(N+1) \rceil$. Our LBA scheme consumes the least number of non-XOR gates, i.e., $N - \lceil \log_2(N+1) \rceil$, when the computation process of all the output bits does not involve auxiliary bits. Thus, we hold $S_N^{lba} \geq N - \lceil \log_2(N+1) \rceil$.

If all output bits require an auxiliary bit for computation, then our LBA scheme consumes the most non-XOR gates. The number of auxiliary bits is $\lceil \log_2(N+1) \rceil$, and the number of non-XOR gates added as a result is also $\lceil \log_2(N+1) \rceil$. The total number of non-XOR gates for this case is $N - \lceil \log_2(N+1) \rceil + \lceil \log_2(N+1) \rceil = N$. Therefore, we have $S_N^{lba} \leq N$.

The proof is completed. \square

6 BINARIZED NETWORK STRUCTURE CUSTOMIZATION AND OPTIMIZATION

It should be stated that our binarized network customization and optimization are both generalized. In this section, to illustrate them specifically, we instantiate our binarized network with the RNA function prediction which is in the bioinformatics field. Section 6.1 describes the process of customizing the target CNN to a binarized network structure. Section 6.2 shows how to transform a binarized network structure while maintaining approximately the same cost.

6.1 Customized Binarized Model

The application of deep learning in the field of bioinformatics has gradually emerged in the past few years. We consider an RNA function prediction scenario from the paper [20]. In such a scenario, a standard deep learning CNN architecture to predict short non-coding RNA functions from only raw sequence data is proposed. According to the dimension of the convolutional layers, we divided the model into two types, 1D and 2D. The convolutional network architectures we adopted are presented in Table 6. The models work, but they don't take the privacy of the data and the security of the computation into account. In order to achieve the secure prediction of CNN for short non-coding RNA functions, we binarize the architectures by following the principles depicted in Section 3 to make binarized networks more suitable for the operations of secure computation.

Customized Convolution: We binarize the weights of the convolutional layers and discard the bias, and we increase the number of filters to compensate for the loss of precision caused by binarization. We keep the kernel size constant for 2D and increase it to 10 for 1D.

Customized Activation: Rectified linear unit (ReLU) activation works well with arithmetic over floating-point numbers. However, fixed-point arithmetic is generally used in secure multiparty computation. Thus, we replace it with Sign activation. In addition, we incorporate a batch normalization layer before each activation layer for efficient secure computation.

Customized Max-pooling and Full-Connected: We keep the parameters consistent with the original convolutional network architecture.

We also add two binarized convolutional layers to achieve the original accuracy. Table 7 describes the relevant parameters of our binarized network architectures.

6.2 Network Structure Optimization

In this section, we explore modifying different network structures while consuming approximate costs (i.e., the number of non-XOR gates) with a negligible disparity for oblivious inference using our LBA. Taking the 1D convolution as an example, if the input shape of a binarized convolutional layer is $m \times n$, there are 128 filters, and the kernel size is 10. Thus, we can know the output shape is $m \times 128$. We can obtain the cost consumed at this point as $C_{10} = m \cdot 128 \cdot S_{10n}^{lba}$. While keeping the output shape constant, we can split this into two modified binarized convolutional layers, where each layer has 128 filters and a kernel size of 5. Each modified convolutional layer consumes a cost of $C_5 = m \cdot 128 \cdot S_{5n}^{lba}$. We approximately make the equation $S_{10n}^{lba} = 2 \cdot S_{5n}^{lba}$ hold, so we have $C_{10} = 2 \cdot C_5$. We claim that the modified structure and the original structure consume approximately the same cost.

Following the above modifications, we modify three network structures for each binary network shown in Table 8 and Table 9. Specifically, for 1D convolutions, we reduce the kernel size from 10 to 5 to become the first structure (i.e., MN1). The kernel size of the second structure (i.e., MN2) is enlarged to 20. We keep the kernel size constant, increase the number of convolution layers, and use it as the third modified structure (i.e., MN3). In 2D convolutions, we reduce the window of the convolution kernel from 3×3 to 2×2

in MN1 and increase the window to 4×4 in MN2. The window size remains the same (i.e., 3×3), while the number of convolution layers increases in MN3. To maintain the same cost of oblivious inference, the number of convolutional kernels scales with the kernel size.

7 APPLICATION AND EXPERIMENTS

In this section, we first compare our schemes with previous work in terms of convolution operators. Then, we instantiate our binarized network with the RNA function prediction and perform secure inference by using the proposed BLB computation and LBA computation based on our customized binarized neural network model and garbled circuits, compared to the state-of-the-art which uses the tree-adder structure. We evaluate the three schemes on nRC and Rfam datasets. Finally, we evaluate the effect of different binarized network structures at approximately the same cost.

7.1 Evaluation on Convolution Operators

To purely compare the performance of our two proposed schemes with the conventional tree-adder structure in terms of convolution operators, we perform experiments on simulated data. We conduct extensive evaluations and average the results. Table 1 compares our BLB solution and LBA solution with the conventional tree-adder structure (TS) in terms of running time, the number of non-XOR gates, and communication overhead. As can be seen, our BLB reduces the running time by up to 23.2 percent compared to TS, and LBA achieves up to 2.5x faster compared to TS. In terms of the number of non-XOR gates, compared to TS, we can observe that BLB and LBA improve by up to 16.5 percent and 50.4 percent respectively. Furthermore, Table 1 demonstrates that our BLB and LBA save up to 16.5 percent and 50.4 percent of communication overhead compared to TS, respectively.

Table 1: Performance comparison of running time (RT.), non-XOR gates, and communication overhead (Comm.) as the size of a bit vector varies

Size	Approach	RT. (μs)	Non-XOR gates	Comm. (KB)
250	TS	59	492	15.38
	BLB	47	412	12.84
	LBA	28	244	7.63
500	TS	110	992	30.97
	BLB	90	832	25.91
	LBA	48	496	15.44
1000	TS	224	1992	62.19
	BLB	172	1664	51.97
	LBA	89	996	31.06
2000	TS	446	3992	124.66
	BLB	351	3340	104.31
	LBA	185	1996	62.31

7.2 Experimental Settings

Our binarized neural network architecture for the RNA function prediction is depicted in Figure 8. The raw RNA sequences are first encoded into an input layer representation of 1D (resp. 2D) by k -mer encoding (resp. space-filling curve) with the *new* padding criteria [20], then up to the binarized network. The network is

composed of five convolution (CONV) layers, each composed of a batch normalization layer, a binary activation function, and a max-pooling (MP) layer if necessary. Finally, one dense layer of Sign is added to reduce the data dimension to a softmax multi-class classification output layer.

Fundamental operations in each of the aforementioned layers can be converted to secure arithmetic over fixed-point numbers to perform computation by using the techniques of standard garbled circuits [7, 15]. We train our binarized network using the standard BNN training algorithm [4]. The training codes are implemented in Python using the Tensorflow Library [1]. We evaluate our models on the nRC and Rfam databases, which are two classification benchmarks used in prior work [20]. The oblivious inference operations are implemented based on the emp-toolkit [28], which is a standard C++-based library for garbled circuit computation. Evaluations are performed on a Ubuntu 18.04 LTS machine with 16GB of RAM. Consistent with prior frameworks, we evaluate the benchmarks in the LAN setting. In our experiments, we focus on the following performance metrics: *accuracy*, *running time*, and *communication overhead*.

7.3 Evaluation on nRC and Rfam

We conduct our evaluations on two real bioinformatics datasets nRC and Rfam. The nRC dataset is a publicly available dataset of ncRNA sequences distributed among 13 functional macro-classes. After data processing, it ended up containing 6,160 RNA sequences for training, and 2,529 RNA sequences for testing. The Rfam dataset is a novel dataset composed of sequences distributed among 88 different Rfam classes. It consists of 105,864 training items, 17,324 validation items, and 25,342 testing items. We consider three types of 1D k -mer encoding (resp. 2D space-filling curves): 3mer, 2mer, and 1mer (resp. Snake, Morton, and Hilbert). Due to the size of the data, we set the window of the second and the fourth max-pooling layers in the binarized network to 4 in 1D k -mer encoding for the nRC dataset.

First of all, we do a performance comparison between the ncna-deep model [20] and our customized binarized neural network (CBN) model. Table 2 shows the accuracy of two models on two datasets. As can be seen, in terms of nRC database, our solution achieves higher accuracy compared to ncna-deep, and the accuracy of 2D increases more than that of 1D. It indicates that our binarized network can match or even exceed the accuracy of the initial convolutional neural network. We can observe from Table 2 that our CBN is superior to ncna-deep, except for 3-mer encoding and 2-mer encoding in the Rfam dataset.

We then perform secure inference for our binarized network using LBA based on our CBN. To analyze the running time and the communication overhead, we implement the secure inference of ncna-deep and our CBN using garbled circuits, and the comparison results are summarized in Table 3. We can observe that the running time and the communication overhead of our secure scheme are much less than that of ncna-deep. It reflects the effectiveness of customizing binarized networks for oblivious inference.

Table 4 compares the performance of our framework which uses BLB solution and LBA solution with the prior art in terms of total running time, total communication overhead, and the number of

Table 2: Accuracy (Acc.) comparison between ncna-deep and our customized binarized network (CBN) for two datasets

Dimension	Encoding	Framework	Acc. (%)	
			nRC	Rfam
1D	3mer	ncna-deep	81.61	86.43
		CBN	82.96	84.93
	2mer	ncna-deep	85.01	87.63
		CBN	85.65	86.88
	1mer	ncna-deep	85.69	89.24
		CBN	87.66	90.14
2D	Snake	ncna-deep	78.88	81.04
		CBN	88.06	81.19
	Morton	ncna-deep	79.52	81.12
		CBN	87.35	81.58
	Hilbert	ncna-deep	80.27	80.21
		CBN	86.00	81.62

Table 3: Running time (RT.) and communication overhead (Comm.) comparison of oblivious inference for the nRC and Rfam datasets

Encoding	Framework	RT. (s)		Comm. (MB)	
		nRC	Rfam	nRC	Rfam
3mer	secure ncna-deep	47.42	12.20	37281	9868
	secure CBN	10.25	2.95	4290	1303
2mer	secure ncna-deep	51.25	13.58	41196	11010
	secure CBN	7.20	2.35	3155	1141
1mer	secure ncna-deep	93.75	24.70	75051	19884
	secure CBN	9.93	3.96	4770	1922
Snake	secure ncna-deep	86.34	19.01	70479	16166
	secure CBN	22.05	5.23	9735	2426
Morton	secure ncna-deep	113.44	28.20	92624	23511
	secure CBN	28.08	6.38	12851	3072
Hilbert	secure ncna-deep	114.85	27.67	92624	23511
	secure CBN	27.49	6.35	12851	3072

non-XOR gates consumed in oblivious inference. It should be noted that the performance evaluation of oblivious inference involves the whole FOBNN, of which our BLB and LBA algorithms are only a part. Thus, in terms of overall performance, the number of non-XOR gates consumed when using the LBA architecture is not always half of what it is when using the XONN architecture.

In summary, compared to XONN in the nRC database, our BLB solution reduces the total running time by up to 24.7 percent and 24.8 percent in 1D k -mer encoding and 2D space-filling curves respectively. Our LBA solution achieves up to 3.4 \times and 3.6 \times faster inference in 1D k -mer encoding and 2D space-filling curves respectively. As can be seen, BLB and LBA reduce the communication overhead by up to 15.2 and 45.5 percent in 1D k -mer encoding, and 15.8 and 47.8 percent in 2D space-filling curves, respectively. Furthermore, the table shows the number of non-XOR gates consumed in all layers. Our BLB solution achieves up to 15.2 percent (resp. 15.8 percent) reduction compared to XONN in 1D k -mer encoding (resp. 2D space-filling curves), and LBA reduces by up to 45.5 percent (resp. 47.8 percent) in 1D k -mer encoding (resp. 2D space-filling curves).

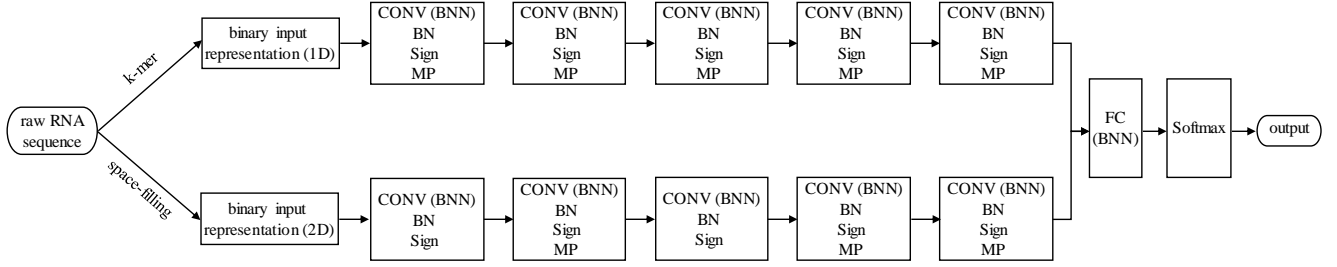


Figure 8: Binarized model architecture for the RNA function prediction.

Table 4: Total running time (TRT.), total communication overhead (TCO.), and number of non-XOR gates (GNum.) for oblivious inference of three architectures for the nRC and Rfam datasets

Dimension	Encoding	Architecture	nRC			Rfam		
			TRT. (s)	TCO. (MB)	GNum	TRT. (s)	TCO. (MB)	GNum
1D	3mer	XONN	18.94	5730	187761396	5.99	1788	58592164
		BLB	15.44	5103	167586356	4.84	1593	52192612
		LBA	10.25	4290	140581256	2.95	1303	42696116
	2mer	XONN	18.74	5140	168429948	7.08	1886	61808552
		BLB	14.75	4435	145328012	5.22	1628	53361848
		LBA	7.20	3155	103367556	2.35	1141	37389492
	1mer	XONN	33.81	8758	286969472	13.41	3538	115919404
		BLB	25.46	7427	243371292	10.53	3003	98407752
		LBA	9.93	4770	156297100	3.96	1922	62978744
2D	Snake	XONN	76.55	18654	611257096	17.09	4540	148762808
		BLB	57.56	15701	514492844	12.93	3839	125784984
		LBA	22.05	9735	319011984	5.23	2426	79490992
	Morton	XONN	99.44	24635	807247744	22.06	5794	189841972
		BLB	76.12	20734	679402280	16.88	4892	160306976
		LBA	28.08	12851	421116312	6.38	3072	100651068
	Hilbert	XONN	100.35	24635	807247744	22.07	5794	189841972
		BLB	75.74	20734	679402280	17.06	4892	160306976
		LBA	27.49	12851	421116312	6.35	3072	100651068

As can be seen in the Rfam database, in terms of the total running time, our BLB solution is up to 26.3 percent and 24.3 percent faster than XONN in 1D *k*-mer encoding and 2D space-filling curves respectively, and LBA achieves up to 3.4× and 3.5× better latency compared to XONN respectively. We can observe that BLB and LBA reduce the communication overhead by up to 15.1 and 45.7 percent in 1D *k*-mer encoding, and 15.6 and 47.0 percent in 2D space-filling curves, respectively. Besides, the number of non-XOR gates consumed in oblivious inference for three schemes is shown in the table. In summary, our BLB solution and LBA solution improve by up to 15.6 percent and 47.0 percent compared to XONN in 1D *k*-mer encoding and 2D space-filling curves.

7.4 Binarized Network Structure Optimization

To compare the performance of different network architectures at approximately the same cost, we retrain the modified networks and perform secure inference. Table 5 presents the comparison of the accuracy of four network structures while performing oblivious inference at the same cost. We first analyze the results of 1D convolutions. As can be seen, when the second dimension of the

input shape for each sample is relatively large, CBN has the best performance, and the performance of MN1 is approximately equal to that of CBN. Therefore, in this case, we suggest that the accuracy in secure inference can be improved by maintaining the same kernel size as the CNN while increasing the number of convolution layers. We can also observe that in the case of a huge difference in the size of the two dimensions (i.e., 2mer and 1mer encodings), MN1 is superior to other network structures. This suggests that in such cases, the kernel size should be reduced and the depth of the network should be appropriately increased in the design of the binarization network structure to achieve the optimal effect. However, in the 1mer encoding of the Rfam dataset, where the second dimension of the input is small and the gap to the first dimension is relatively small, the CBN performs best. This illustrates that binarized network structures need to be designed elaborately.

Table 5 also shows the comparison results for 2D convolutions. CBN and MN3 outperform other network architectures regardless of variations in the input pixels and encoding methods. This means that for 2D convolutions, the convolution window should be kept the same as the window of the original CNN for more efficient

binarization. When the input pixels are larger, we can increase the number of convolutional layers as little as possible to achieve optimal performance. For smaller input pixels, we can try to appropriately increase the depth of the network to improve the accuracy of oblivious inference. Therefore, we recommend that to obtain the best accuracy for secure inference, it is better to set the window of the convolution kernel to be the same as the unbinarized CNN, which performs best, and elaborately design the binarized network structure.

As can be seen in Table 5, the running time and communication overheads of the four network architectures are also not very different (i.e., within acceptable limits), which also satisfies the condition of approximate equality of costs for oblivious inference. Therefore, we propose to balance accuracy, runtime, and communication overhead for different application focuses to select the most appropriate network structure.

8 RELATED WORK

CryptoNets [8] proposes a practical method using homomorphic encryption to perform oblivious inference. CryptoNets combines cryptography, machine learning, and engineering to achieve secure inference while maintaining high throughput and accuracy. SecureML [19] presents new and efficient protocols for privacy-preserving machine learning for linear regression, logistic regression, and neural networks based on garbled circuits and secret sharing. SecureML also implements the first privacy-preserving system for training neural networks. Since then, some solutions for secure neural network inference have been proposed which are based on secret sharing (SS) and homomorphic encryption (HE) such as ABY3 [18], SecureNN [26], Falcon [27], CHET [6], AutoPrivacy [17], CryptFlow2 [22] and others [3].

DeepSecure [25] presents a provably secure deep learning framework. The secure computation in DeepSecure is performed using Yao's GC protocol. The privacy of network parameters and data structures can not be guaranteed in DeepSecure. Several hybrid protocols for oblivious reasoning have emerged. MiniONN [16] proposes an approach for transforming an existing neural network to an oblivious neural network based on GC, SS, and HE, and it supports privacy-preserving predictions with reasonable efficiency. Gazelle [12] is a low-latency framework for secure neural network inference, which uses mixed protocols that rely on GC and additive HE. Chameleon [24] utilizes GC and SS to achieve a novel mixed-protocol framework for secure function evaluation. These hybrid protocols are not constant rounds of complexity, and they are not deep learning-secure computation co-design approaches. XONN [23] is the first work to combine GC with binary networks to perform XNOR-based oblivious inference, where the XNOR operations in BNNs can be evaluated for free in GC. They provide a more efficient solution compared to mixed-protocol solutions. However, they did not take into account the conversion of costly operations in neural networks to take full advantage of the computational characteristics of GC. Compared to prior work, we consider the optimization of neural networks while implementing oblivious inference based on BNNs, that is, the computationally expensive convolution and linear operations are optimized into GC-compatible alternatives.

There is also a line of work on secure inference solutions for QNNs with secret sharing, such as QUOTIENT [2], SecureQNN [5]. Banners [10] and SecureBiNN [32] present three-party secure computations for binarized neural network inference with the replicated secret sharing technique. Zhang *et al.* [31] study the application of binary neural networks in oblivious inference based on GC and additive SS. However, secure inference with secret sharing is not the goal of our work.

9 CONCLUSION

We introduce FOBNN, a novel framework for oblivious binarized network inference. Our FOBNN customizes the binarized networks and optimizes the operations to be GC-compatible alternatives. To address the costly convolutional computation using GC in BNNs, we propose a Bit Length Bounding approach and a Layer-wise Bit Accumulation approach for fast computation, which require less running time and fewer non-XOR gates. We theoretically analyze the advantages of our two solutions compared to the tree-adder structure. Furthermore, we modify different network structures while maintaining the same cost of oblivious inference to perform network structure optimization exploration. Finally, we implement our solutions in a bioinformatics scenario, and extensive experimental results show that the performance of our solutions is superior to prior art. By comparing the performance of different network architectures, we provide our recommendations for network optimization.

REFERENCES

- [1] Martin Abadi, Paul Barham, Jianmin Chen, Zhifeng Chen, Andy Davis, Jeffrey Dean, Matthieu Devin, Sanjay Ghemawat, Geoffrey Irving, Michael Isard, et al. 2016. TensorFlow: a system for large-scale machine learning. In *12th USENIX symposium on operating systems design and implementation (OSDI 16)*. 265–283.
- [2] Nitin Agrawal, Ali Shahin Shamsabadi, Matt J Kusner, and Adrià Gascón. 2019. QUOTIENT: two-party secure neural network training and prediction. In *Proceedings of the 2019 ACM SIGSAC Conference on Computer and Communications Security*. 1231–1247.
- [3] Alon Brutzkus, Ran Gilad-Bachrach, and Oren Elisha. 2019. Low latency privacy preserving inference. In *International Conference on Machine Learning*. PMLR, 812–821.
- [4] Matthieu Courbariaux, Itay Hubara, Daniel Soudry, Ran El-Yaniv, and Yoshua Bengio. 2016. Binarized neural networks: Training deep neural networks with weights and activations constrained to +1 or -1. *arXiv preprint arXiv:1602.02830* (2016).
- [5] Anders Dalskov, Daniel Escudero, and Marcel Keller. 2020. Secure Evaluation of Quantized Neural Networks. *Proceedings on Privacy Enhancing Technologies 4* (2020), 355–375.
- [6] Roshan Dathathri, Olli Saarikivi, Hao Chen, Kim Laine, Kristin Lauter, Saeed Maleki, Madanlal Musuvathi, and Todd Mytkowicz. 2019. CHET: an optimizing compiler for fully-homomorphic neural-network inferencing. In *Proceedings of the 40th ACM SIGPLAN conference on programming language design and implementation*. 142–156.
- [7] David Evans, Vladimir Kolesnikov, Mike Rosulek, et al. 2018. A pragmatic introduction to secure multi-party computation. *Foundations and Trends® in Privacy and Security 2*, 2-3 (2018), 70–246.
- [8] Ran Gilad-Bachrach, Nathan Dowlin, Kim Laine, Kristin Lauter, Michael Naehrig, and John Wernsing. 2016. Cryptonets: Applying neural networks to encrypted data with high throughput and accuracy. In *International conference on machine learning*. PMLR, 201–210.
- [9] Itay Hubara, Matthieu Courbariaux, Daniel Soudry, Ran El-Yaniv, and Yoshua Bengio. 2018. Quantized neural networks: Training neural networks with low precision weights and activations. *journal of machine learning research 18*, 187 (2018), 1–30.
- [10] Alberto Ibarrondo, Hervé Chabanne, and Melek Önen. 2021. Banners: Binarized neural networks with replicated secret sharing. In *Proceedings of the 2021 ACM Workshop on Information Hiding and Multimedia Security*. 63–74.
- [11] Sergey Ioffe and Christian Szegedy. 2015. Batch normalization: Accelerating deep network training by reducing internal covariate shift. In *International conference*

Table 5: Accuracy, runtime, communication comparison of different modified architectures while maintaining the cost in oblivious inference

Encoding	Input	Accuracy (%)				Runtime (s)				Comm. (MB)			
		CBN	MN1	MN2	MN3	CBN	MN1	MN2	MN3	CBN	MN1	MN2	MN3
3mer(nRC)	257×65	82.96	82.44	81.34	80.43	10.25	10.59	9.79	10.31	4290	4364	4215	4299
2mer(nRC)	385×17	85.65	86.00	80.55	84.34	7.20	6.92	6.56	7.04	3155	3243	3066	3160
1mer(nRC)	770×5	87.66	88.22	83.04	87.54	9.93	9.90	8.81	10.19	4770	4890	4677	4805
3mer(Rfam)	67×65	84.93	84.80	82.22	83.60	2.95	3.11	2.88	3.04	1303	1366	1229	1306
2mer(Rfam)	100×17	86.88	88.11	85.54	87.00	2.35	2.49	2.28	2.36	1141	1210	1047	1146
1mer(Rfam)	200×5	90.14	89.77	88.94	89.11	3.96	4.02	3.56	4.12	1922	2001	1815	1933
Snake(nRC)	28×28×5	88.06	83.79	84.86	86.71	22.05	18.76	18.42	21.49	9735	9213	8827	9802
Morton(nRC)	32×32×5	87.35	80.78	83.99	84.97	28.08	25.28	24.27	28.42	12851	12136	11696	12939
Hilbert(nRC)	32×32×5	86.00	82.09	83.12	86.12	27.49	25.27	23.97	28.74	12851	12136	11696	12939
Snake(Rfam)	15×15×5	81.19	83.90	82.85	84.24	5.23	4.78	4.53	5.27	2426	2337	2168	2443
Morton(Rfam)	16×16×5	81.58	78.83	79.30	81.28	6.38	6.27	5.91	6.57	3072	2950	2733	3093
Hilbert(Rfam)	16×16×5	81.62	80.95	81.40	82.21	6.35	6.17	5.96	6.49	3072	2950	2733	3093

on machine learning. pmlr, 448–456.

[12] Chiraag Juvekar, Vinod Vaikuntanathan, and Anantha Chandrakasan. 2018. GAZELLE: A low latency framework for secure neural network inference. In *27th USENIX Security Symposium (USENIX Security 18)*. 1651–1669.

[13] Vladimir Kolesnikov, Ahmad-Reza Sadeghi, and Thomas Schneider. 2009. Improved garbled circuit building blocks and applications to auctions and computing minima. In *Cryptography and Network Security: 8th International Conference, CANS 2009, Kanazawa, Japan, December 12–14, 2009. Proceedings 8*. Springer, 1–20.

[14] Vladimir Kolesnikov and Thomas Schneider. 2008. Improved garbled circuit: Free XOR gates and applications. In *Automata, Languages and Programming: 35th International Colloquium, ICALP 2008, Reykjavik, Iceland, July 7–11, 2008. Proceedings, Part II 35*. Springer, 486–498.

[15] Yehuda Lindell and Benny Pinkas. 2009. A proof of security of Yao’s protocol for two-party computation. *Journal of cryptology* 22 (2009), 161–188.

[16] Jian Liu, Mika Juuti, Yao Lu, and Nadarajah Asokan. 2017. Oblivious neural network predictions via minion transformations. In *Proceedings of the 2017 ACM SIGSAC conference on computer and communications security*. 619–631.

[17] Qian Lou, Song Bian, and Lei Jiang. 2020. Autoprivacy: Automated layer-wise parameter selection for secure neural network inference. *Advances in Neural Information Processing Systems* 33 (2020), 8638–8647.

[18] Payman Mohassel and Peter Rindal. 2018. ABY3: A mixed protocol framework for machine learning. In *Proceedings of the 2018 ACM SIGSAC conference on computer and communications security*. 35–52.

[19] Payman Mohassel and Yupeng Zhang. 2017. Secureml: A system for scalable privacy-preserving machine learning. In *2017 IEEE symposium on security and privacy (SP)*. IEEE, 19–38.

[20] Teresa Maria Rosaria Noviello, Francesco Ceccarelli, Michele Ceccarelli, and Luigi Cerulo. 2020. Deep learning predicts short non-coding RNA functions from only raw sequence data. *PLoS computational biology* 16, 11 (2020), e1008415.

[21] Michael O Rabin. 2005. How to exchange secrets with oblivious transfer. *Cryptology ePrint Archive* (2005).

[22] Deevashwer Rathee, Mayank Rathee, Nishant Kumar, Nishanth Chandran, Divya Gupta, Aseem Rastogi, and Rahul Sharma. 2020. Cryptflow2: Practical 2-party secure inference. In *Proceedings of the 2020 ACM SIGSAC Conference on Computer and Communications Security*. 325–342.

[23] M Sadegh Riazi, Mohammad Samragh, Hao Chen, Kim Laine, Kristin Lauter, and Farinaz Koushanfar. 2019. XONN: XNOR-based oblivious deep neural network inference. In *28th USENIX Security Symposium (USENIX Security 19)*. 1501–1518.

[24] M Sadegh Riazi, Christian Weinert, Oleksandr Tkachenko, Ebrahim M Songhori, Thomas Schneider, and Farinaz Koushanfar. 2018. Chameleon: A hybrid secure computation framework for machine learning applications. In *Proceedings of the 2018 Asia conference on computer and communications security*. 707–721.

[25] Bitar Darvish Rouhani, M Sadegh Riazi, and Farinaz Koushanfar. 2018. Deepsecure: Scalable provably-secure deep learning. In *Proceedings of the 55th annual design automation conference*. 1–6.

[26] Sameer Wagh, Divya Gupta, and Nishanth Chandran. 2019. SecureNN: 3-Party Secure Computation for Neural Network Training. *Proc. Priv. Enhancing Technol.* 2019, 3 (2019), 26–49.

[27] Sameer Wagh, Shruti Tople, Fabrice Benhamouda, Eyal Kushilevitz, Prateek Mittal, and Tal Rabin. 2021. Falcon: Honest-Majority Maliciously Secure Framework for Private Deep Learning. *Proceedings on Privacy Enhancing Technologies* 1 (2021), 188–208.

[28] Xiao Wang, Alex J. Malozemoff, and Jonathan Katz. 2016. EMP-toolkit: Efficient MultiParty computation toolkit. <https://github.com/emp-toolkit>.

[29] Jiayang Wu, Cong Leng, Yuhang Wang, Qinghao Hu, and Jian Cheng. 2016. Quantized convolutional neural networks for mobile devices. In *Proceedings of the IEEE conference on computer vision and pattern recognition*. 4820–4828.

[30] Andrew Chi-Chih Yao. 1986. How to generate and exchange secrets. In *27th annual symposium on foundations of computer science (Sfcs 1986)*. IEEE, 162–167.

[31] Xinqiao Zhang, Mohammad Samragh, Siam Hussain, Ke Huang, and Farinaz Koushanfar. 2023. Scalable Binary Neural Network applications in Oblivious Inference. *ACM Transactions on Embedded Computing Systems* (2023).

[32] Wenxing Zhu, Mengqi Wei, Xiangxue Li, and Qiang Li. 2022. Securebinn: 3-party secure computation for binarized neural network inference. In *European Symposium on Research in Computer Security*. Springer, 275–294.

A DERIVATION DETAILS

A.1 The Derivation of S_N^{ts}

We hold $S_N^{ts} = \sum_{\ell=1}^L (\frac{N}{2^\ell} \cdot \ell)$ so that we can obtain the following computational procedure.

$$S_N^{ts} = \sum_{\ell=1}^L (\frac{N}{2^\ell} \cdot \ell) = 1 \cdot \frac{N}{2} + 2 \cdot \frac{N}{2^2} + 3 \cdot \frac{N}{2^3} + \dots + L \cdot \frac{N}{2^L} \quad (4)$$

Multiplying both sides of (4) by $\frac{1}{2}$ yields the following equation.

$$\frac{1}{2} S_N^{ts} = 1 \cdot \frac{N}{2^2} + 2 \cdot \frac{N}{2^3} + 3 \cdot \frac{N}{2^4} + \dots + L \cdot \frac{N}{2^{L+1}} \quad (5)$$

Equation (4) minus (5):

$$S_N^{ts} - \frac{1}{2} S_N^{ts} = \frac{N}{2} + \frac{N}{2^2} + \frac{N}{2^3} + \dots + \frac{N}{2^L} - L \cdot \frac{N}{2^{L+1}} \quad (6)$$

We hold $L = \log_2 N$. Equation (5) can be simplified as follows.

$$\frac{1}{2} S_N^{ts} = \frac{N}{2} + \frac{N}{2^2} + \frac{N}{2^3} + \dots + \frac{N}{2^{\log_2 N}} - \log_2 N \cdot \frac{N}{2^{\log_2 N+1}}$$

$$S_N^{ts} = N \cdot \left(1 + \frac{1}{2} + \frac{1}{2^2} + \dots + \frac{1}{2^{\log_2 N-1}}\right) - \log_2 N$$

$$S_N^{ts} = N \cdot 2 \cdot \frac{N-1}{N} - \log_2 N$$

$$S_N^{ts} = 2 \cdot (N-1) - \log_2 N$$

Equation (1) is derived.

A.2 The Derivation of G_K

In each group, the input of the computation are 2^K -bit numbers and the output is a 2^{K+1} -bit number. The first $2^{2^K} + 1$ numbers are computed using an inverted binary tree structure. In the tree, the number of ℓ -bit adders ($\ell \in [2^K..2^{K+1} - 1]$) is $2^{2^{K+1}-1-\ell}$. Thus, the total number of non-XOR gates for the first $2^{2^K} + 1$ numbers can be computed as follows.

$$S_t = \sum_{\ell=2^K}^{2^{K+1}-1} (2^{2^{K+1}-1-\ell} \cdot \ell) \quad (7)$$

$$= 2^{2^K-1} \cdot 2^K + 2^{2^K-2} \cdot (2^K + 1) + \dots + 2^0 \cdot (2^{K+1} - 1)$$

Multiplying both sides of (7) by $\frac{1}{2}$ yields the following equation.

$$\frac{1}{2}S_t = 2^{2^K-2} \cdot 2^K + 2^{2^K-3} \cdot (2^K + 1) + \dots + 2^1 \cdot (2^{K+1} - 1) \quad (8)$$

Equation (7) minus (8):

$$S_t - \frac{1}{2}S_t$$

$$= 2^{2^K-1} \cdot 2^K + 2^{2^K-2} + 2^{2^K-3} + \dots + 1 - \frac{1}{2} \cdot (2^{K+1} - 1) \quad (9)$$

Equation (9) can be simplified as follows.

$$S_t = 2^{2^K} \cdot 2^K + (2^{2^K-1} + 2^{2^K-2} + \dots + 2) - (2^{K+1} - 1)$$

$$= 2^{2^K} \cdot 2^K + 2 \cdot \frac{1 - 2^{2^K-1}}{1 - 2} - 2^{K+1} + 1$$

$$= 2^{2^K} \cdot 2^K + 2^{2^K} - 2^{K+1} - 1$$

The sum of the first $2^{2^K} + 1$ numbers produces a 2^{K+1} -bit number. The non-XOR gates generated by summing this number with the remaining 2^K -bit number also needs to be computed.

$$G_K = S_t + (2^{K+1} - 1) = 2^{2^K} \cdot 2^K + 2^{2^K} - 2$$

Equation (3) is derived.

B MODEL DETAILS

Table 6: Convolutional Network Architecture of 1D and 2D

1D	
1	CONV[filters:32, kernel_size:3] + ReLU
2	MP[pool_size:2]
3	CONV[filters:64, kernel_size:3] + ReLU
4	MP[pool_size:2]
5	CONV[filters:128, kernel_size:3] + ReLU
6	MP[pool_size:2]
7	FC[output:130] + ReLU
2D	
1	CONV>window:3×3, kernels:32s + ReLU
2	MP>window:2×2
3	CONV>window:3×3, kernels:64s + ReLU
4	MP>window:2×2
5	CONV>window:3×3, kernels:128s + ReLU
6	MP>window:2×2
7	FC[output:130] + ReLU

Table 7: Binarized Network Architecture of 1D and 2D

1D	
1	CONV (BNN)[filters:128,kernel_size:10] + BN + Sign
2	MP[pool_size:2]
3	CONV (BNN)[filters:128,kernel_size:10] + BN + Sign
4	MP[pool_size:2]
5	CONV (BNN)[filters:256,kernel_size:10] + BN + Sign
6	MP[pool_size:2]
7	CONV (BNN)[filters:256,kernel_size:10] + BN + Sign
8	MP[pool_size:2]
9	CONV (BNN)[filters:256,kernel_size:10] + BN + Sign
10	MP[pool_size:2]
11	FC (BNN)[output:130] + BN + Sign
2D	
1	CONV (BNN)[window:3×3,kernels:128s] + BN + Sign
2	CONV (BNN)[window:3×3,kernels:128s] + BN + Sign
3	MP>window:2×2
4	CONV (BNN)[window:3×3,kernels:256s] + BN + Sign
5	CONV (BNN)[window:3×3,kernels:256s] + BN + Sign
6	MP>window:2×2
7	CONV (BNN)[window:3×3,kernels:256s] + BN + Sign
8	MP>window:2×2
9	FC (BNN)[output:130] + BN + Sign

Table 9: Modified Network Architectures of 2D

MN1 for 2D	
1	CONV (BNN)[window:3×3,kernels:128s] + BN + Sign
2	CONV (BNN)[window:2×2,kernels:128s] + BN + Sign
3	CONV (BNN)[window:2×2,kernels:128s] + BN + Sign
4	MP>window:2×2]
5	CONV (BNN)[window:3×3,kernels:256s] + BN + Sign
6	CONV (BNN)[window:2×2,kernels:256s] + BN + Sign
7	CONV (BNN)[window:2×2,kernels:256s] + BN + Sign
8	MP>window:2×2]
9	CONV (BNN)[window:2×2,kernels:256s] + BN + Sign
10	CONV (BNN)[window:2×2,kernels:256s] + BN + Sign
11	MP>window:2×2]
12	FC (BNN)[output:130] + BN + Sign
MN2 for 2D	
1	CONV (BNN)[window:3×3,kernels:128s] + BN + Sign
2	CONV (BNN)[window:3×3,kernels:128s] + BN + Sign
3	MP>window:2×2]
4	CONV (BNN)[window:4×4,kernels:128s] + BN + Sign
5	CONV (BNN)[window:4×4,kernels:256s] + BN + Sign
6	MP>window:2×2]
7	CONV (BNN)[window:4×4,kernels:64s] + BN + Sign
8	CONV (BNN)[window:4×4,kernels:256s] + BN + Sign
9	MP>window:2×2]
10	FC (BNN)[output:130] + BN + Sign
MN3 for 2D	
1	CONV (BNN)[window:3×3,kernels:128s] + BN + Sign
2	CONV (BNN)[window:3×3,kernels:64s] + BN + Sign
2	CONV (BNN)[window:3×3,kernels:128s] + BN + Sign
4	MP>window:2×2]
5	CONV (BNN)[window:3×3,kernels:256s] + BN + Sign
6	CONV (BNN)[window:3×3,kernels:128s] + BN + Sign
7	CONV (BNN)[window:3×3,kernels:256s] + BN + Sign
6	MP>window:2×2]
7	CONV (BNN)[window:3×3,kernels:128s] + BN + Sign
8	CONV (BNN)[window:3×3,kernels:256s] + BN + Sign
9	MP>window:2×2]
10	FC (BNN)[output:130] + BN + Sign

Table 8: Modified Network Architectures of 1D

MN1 for 1D	
1	CONV (BNN)[filters:128,kernel_size:10] + BN + Sign
2	MP[pool_size:2]
3	CONV (BNN)[filters:128,kernel_size:5] + BN + Sign
4	CONV (BNN)[filters:128,kernel_size:5] + BN + Sign
5	MP[pool_size:2]
6	CONV (BNN)[filters:256,kernel_size:10] + BN + Sign
7	MP[pool_size:2]
8	CONV (BNN)[filters:256,kernel_size:5] + BN + Sign
9	CONV (BNN)[filters:256,kernel_size:5] + BN + Sign
10	MP[pool_size:2]
11	CONV (BNN)[filters:256,kernel_size:5] + BN + Sign
12	CONV (BNN)[filters:256,kernel_size:5] + BN + Sign
13	MP[pool_size:2]
14	FC (BNN)[output:130] + BN + Sign
MN2 for 1D	
1	CONV (BNN)[filters:128,kernel_size:10] + BN + Sign
2	MP[pool_size:2]
3	CONV (BNN)[filters:32,kernel_size:20] + BN + Sign
4	CONV (BNN)[filters:128,kernel_size:20] + BN + Sign
5	MP[pool_size:2]
6	CONV (BNN)[filters:256,kernel_size:10] + BN + Sign
7	MP[pool_size:2]
8	CONV (BNN)[filters:64,kernel_size:20] + BN + Sign
9	CONV (BNN)[filters:256,kernel_size:20] + BN + Sign
10	MP[pool_size:2]
11	CONV (BNN)[filters:64,kernel_size:20] + BN + Sign
12	CONV (BNN)[filters:256,kernel_size:20] + BN + Sign
13	MP[pool_size:2]
14	FC (BNN)[output:130] + BN + Sign
MN3 for 1D	
1	CONV (BNN)[filters:128,kernel_size:10] + BN + Sign
2	MP[pool_size:2]
3	CONV (BNN)[filters:64,kernel_size:10] + BN + Sign
4	CONV (BNN)[filters:128,kernel_size:10] + BN + Sign
5	MP[pool_size:2]
6	CONV (BNN)[filters:256,kernel_size:10] + BN + Sign
7	MP[pool_size:2]
8	CONV (BNN)[filters:128,kernel_size:10] + BN + Sign
9	CONV (BNN)[filters:256,kernel_size:10] + BN + Sign
10	MP[pool_size:2]
11	CONV (BNN)[filters:128,kernel_size:10] + BN + Sign
12	CONV (BNN)[filters:256,kernel_size:10] + BN + Sign
13	MP[pool_size:2]
14	FC (BNN)[output:130] + BN + Sign